Materials Science & Engineering A 711 (2018) 543–552

Contents lists available at ScienceDirect

Materials Science & Engineering A

journal homepage: www.elsevier.com/locate/msea

The tensile behaviors of vanadium-containing 25Cr-20Ni austenitic stainless steel at temperature between 200 °C and 900 °C

Guodong Hu[a,b], Pei Wang[a,b,*], Dianzhong Li[a,b], Yiyi Li[a,b]

[a] Shenyang National Laboratory for Materials Science, Institute of Metal Research, Chinese Academy of Sciences, 72 Wenhua Road, Shenyang 110016, China
[b] School of Materials Science and Engineering, University of Science and Technology of China, 72 Wenhua Road, Shenyang 110016, China

ARTICLE INFO

Keywords:
Austenitic stainless steel
High-temperature tensile properties
Deformation mechanism
Vanadium-containing
Precipitate

ABSTRACT

The high-temperature tensile behaviors of two 25Cr-20Ni austenitic stainless steels with different V concentration (0 wt% V and 0.3 wt% V, respectively), have been studied at temperature between 200 °C and 900 °C. The ultimate tensile strength of both steels is strong temperature dependent, which decreases slowly first at 200–300 °C, keeps platform then at 300–500 °C and decreases rapidly afterwards from 600 °C to 900 °C. It is caused by the decreasing strain hardening ability, dynamic strain aging and dynamic recovery together with dynamic recrystallization at different temperatures. At higher than 800 °C, the elongation of both steels increases markedly due to the dynamic recovery and dynamic recrystallization. However, because of the deteriorated effects of $M_{23}C_6$ precipitates at grain boundary, the elongation of both steels at 700 °C does not increase despite decreasing strength. Additionally, the addition of 0.3 wt% V decreases the ductility of the material in the temperature range of 800 °C to 900 °C, which is induced by the impeding effects of solute vanadium on dynamic recovery and recrystallization.

1. Introduction

25Cr-20Ni austenitic stainless steels are widely used as important structural materials in advanced nuclear industries and power plants because of their good mechanical properties and corrosion resistance at high temperature [1–3]. As structural materials, the mechanical properties at elevated temperature, such as high temperature strength, creep strength and ductility, are of vital importance. Compared to the costly and time-consuming creep test, high-temperature tensile test is a common method to evaluate the mechanical properties of metal material because its result can play a guiding role in the prediction of creep properties. Therefore, the tensile behaviors of austenitic stainless steels at different temperatures have been widely investigated and interpreted from the perspective of microstructure evolution and deformation mechanism. Byun et al. [4] have studied the deformation mechanisms of 316LN austenitic stainless steel during tensile test performed from −150 °C to 450 °C. The results demonstrate that because of the low stacking fault energy (SFE) of 316LN steel, dislocations are unable to cross-slip when the test temperature is below 200 °C, resulting in formation of large dislocation pile-ups below 200 °C but tangled dislocations above 200 °C. The tensile behaviors of 316LN at temperature from 200 °C to 1000 °C have been investigated by Pei et al. [5]. They point out that the deformation mechanisms of 316LN steel are dislocation sliding and twinning at 400 °C or below, dislocation cross-slipping at 600 °C, dynamic recovery at 700 °C, and dynamic recrystallization (DRX) at 800 °C or above. Michel et al. [6] have studied the deformation mechanisms of 316 austenitic stainless steel during slow tensile tests between 21 °C and 816 °C. The results show that dislocation cell walls are formed by tangled dislocations below ~ $0.5T_m$ while regular sub-boundaries are developed above ~ $0.5T_m$. According to the previous research, the deformation mechanisms of austenitic steels depend on the temperature and chemical composition [7–9].

Except for the deformation mechanism of matrix, the effects of precipitates on the tensile properties of austenitic stainless steels have also attracted much attention. Intergranular fracture often occurs in austenitic steels during the tensile test performing at the temperature higher than $0.5T_m$. Various models have been proposed to understand this phenomenon. Grain boundary sliding mechanism is one of the earliest viewpoints [10–13]. It is believed that the movement of dislocations along the grain boundaries (GBs) induces relative displacements of grains at the two sides of the boundary, which further develop to cavity [14–16]. Rao et al. [17] have pointed out that the crack would be predominantly at 45 degree to tensile axis if the growth of cavity was controlled by grain boundary sliding. Unfortunately, the statistical results show cracks are mostly at 90 degree to the tensile axis. Therefore, the concept that the split of the grain boundary between $M_{23}C_6$

* Corresponding author at: Shenyang National Laboratory for Materials Science, Institute of Metal Research, Chinese Academy of Sciences, 72 Wenhua Road, Shenyang 110016, China.
E-mail address: pwang@imr.ac.cn (P. Wang).

https://doi.org/10.1016/j.msea.2017.11.066
Received 15 August 2017; Received in revised form 14 November 2017; Accepted 16 November 2017
Available online 20 November 2017
0921-5093/

precipitates and matrix induces the intergranular fracture has been proposed when it is found that the temperature range of intergranular fracture is in accordance with the precipitation temperature of $M_{23}C_6$ [18,19]. It is generally accepted that $M_{23}C_6$ carbides at GBs reduce the interfacial strength of grains and significantly deteriorate the ductility of austenitic stainless steels [20–22]. Additionally, Ohmori et al. have found that microvoids are formed adjacent to GB $M_{23}C_6$ precipitates and proposed that the microvoids are induced by cracking of $M_{23}C_6$ precipitates [23]. The effects of MX carbonitrides on the deformation behaviors of austenitic stainless steels at high temperature have also been widely studied [24–27]. The results have indicated that MX precipitates would lead to precipitation hardening and improvement of creep strength. However, most of them focus on the effects of Nb-containing and Ti-containing MX. In contrast, the effects of V-containing MX precipitate are scarce. Recently, the effects of V on the creep properties of an austenitic stainless heat resistant steel have been examined [28]. It is found that the addition of V improves the creep strength at 700 °C significantly by forming V-containing precipitates. However, the effects of V addition on tensile properties of austenitic steels are seldom reported.

Although extensive research on deformation mechanisms of austenitic stainless steels at high temperature has been performed, the effects of matrix substructure and some precipitates that formed in the same temperature range, as well as their synergistic effects, on the tensile properties of a V-containing austenitic stainless steel are not clear. To investigate the synergistic effects of different precipitates, and matrix substructure on the tensile properties of 25Cr-20Ni austenitic stainless steel at different temperatures, a series of tensile tests at temperature from 200 °C to 900 °C have been conducted. The experimental results have been interpreted from the aspect of the evolution of microstructure at different scales.

2. Experiments

The investigated materials were prepared by vacuum induction melting in laboratory and the chemical compositions are shown in Table 1. Two steels were prepared with different V contents: 0 V and 0.3 V. The ~ 25 kg ingots were forged into 45 mm × 45 mm rod at 1150 °C–950 °C firstly. And then the solution heat treatment of the forged rod specimens was carried out at 1100 °C for 1 h followed by water quenching. The samples in solution heat treatment condition were electrolytic etched by 60% nitric acid to observe the initial microstructure by the ZEISS Axio Lab. A1 optical microscope (OM) and ZEISS SUPRA 35 scanning electron microscope (SEM). Rod tensile specimens with diameter of 5 mm and gauge length of 25 mm were prepared according to GB/T 4336-2006 for high temperature tension. The dimensional drawing of tensile sample is shown in Fig. 1. Tensile tests were performed on an MTS E45. 105 machine between 200 °C and 900 °C at interval of 100 °C in air with strain rate of $10^{-4}\,s^{-1}$ before yielding and $1.3 \times 10^{-3}\,s^{-1}$ after yielding. Before high-temperature tensile test, thermal insulation for ten minutes was carried out. When the initial gauge length of the specimen was calibrated with mechanical dents or scribed lines, the specimen always fractured at these marked points at 700 °C and 800 °C. Therefore, the crosshead motion value of the tensile machine was used to evaluate the elongation of the samples at various temperatures.

After tensile test, the microstructure of the sample including the morphology of precipitates was observed by SEM after electrolytic etch.

Table 1
Chemical compositions of experimental steels (wt%).

	C	Si	Mn	Cr	Ni	V	Nb	N
0 V steel	0.056	0.56	1.52	24.44	18.92	–	0.53	0.064
0.3 V steel	0.063	0.89	1.65	23.90	19.48	0.33	0.54	0.077

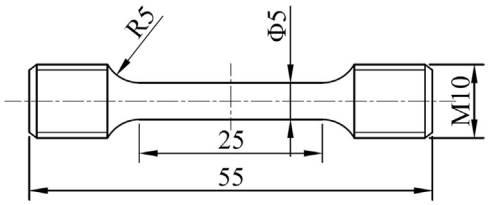

Fig. 1. The dimensional drawing of tensile specimen (mm).

The grain orientation of the sample at the central section parallel to the tensile axis was observed using ZEISS MERLIN COMPACT SEM with Nordlys Nano electron back-scattered diffraction (EBSD) technique. The tensile specimens were cut along the tensile axis to prepare EBSD specimens. The specimens were mechanical polished first and then electropolished in 30% perchloric acid and 70% ethyl alcohol at 45 V and − 20 °C. In EBSD measurement, the step size was adjusted to 600 nm. The GB and grain orientation color maps obtained by EBSD were used to reveal the DRX. The dislocation configuration and precipitates evolution before and after tensile tests at different temperatures were observed using FEI Tecnai F20 Transmission Electron Microscope (TEM). The precipitates were also characterized in high angle annular dark field-scanning transmission electron microscope (HADDF -STEM) images. As HAADF image provides additional information on Z-contrasts, it is an ideal technology to distinguish the precipitates more conveniently. The TEM thin foil specimens were first mechanically polished to thickness of about 50 μm. Subsequently, the foil specimens were electro-polished at − 25 °C with a standard twin jet procedure (TenuPol-5 Struers) using an etching solution of 90% acetic acid and 10% perchloric acid at a voltage of 20 V.

3. Results

3.1. The tensile properties over the test temperature range

Fig. 2(a) presents the ultimate tensile strength (UTS) of the two investigated steels at different temperatures from 200 °C to 900 °C. The two steels have similar UTS in the whole test temperature range. With the test temperature increasing from 200 °C to 300 °C, the UTS of the two steels slightly decreases from ~ 530 MPa to ~ 500 MPa. And then, the UTS remains almost unchanged at ~ 500 MPa as the test temperature increases from 300 °C to 500 °C. At higher temperature, the UTS decreases sharply from ~ 450 MPa at 600 °C to ~ 140 MPa at 900 °C. Fig. 2(b) shows the elongation of the two steels at different test temperatures. From 200 °C to 600 °C, the elongation of both steels keeps almost unchanged with value of ~ 50%. As the test temperature increases to 800 °C and higher, the elongation increases sharply. Contrast to the similar UTS of the two investigated steels at all test temperatures, the elongation of them shows different characteristics. The elongations of them are similar in the temperature range of 200–600 °C. However, when the test temperature increases from 700 °C to 900 °C, the elongation increases from ~ 55% to 120% in 0 V steel and to 100% in 0.3 V steel. That is to say, the V-containing 0.3 V steel has a relatively lower elongation at 800 °C and 900 °C compared to the 0 V steel.

3.2. The initial microstructure of the investigated steels

The SEM micrographs of the two steels in solid solution condition are shown in Fig. 3(a) and (b). The microstructure of both steels is composed of austenitic matrix and dispersively distributed precipitates. Two types of precipitates with different sizes are observed. The larger ones of ~ 5 μ m diameter are primary Nb(C, N) precipitates (indicated by the yellow arrows in Fig. 3(a) and (b)), which are formed in the solidification process and undissolved during the solution heat treatment. The smaller nano-sized MX precipitates (as shown in the inset pictures in Fig. 3(a) and (b)), evenly distributed at GBs and within the